

Hexamethylcyclopentadiene: A test case for the  
combination of time-resolved photoelectron  
spectroscopy and ab initio multiple spawning  
simulations

T. J. A. Wolf<sup>a,b,\*</sup>, T. S. Kuhlman<sup>c</sup>, O. Schalk<sup>d,e</sup>, T. J. Martínez<sup>b,f</sup>,  
K. B. Møller<sup>c</sup>, A. Stolow<sup>e</sup>, A.-N. Unterreiner<sup>a,\*</sup>

**Electronic Supplementary Information**

## Synthesis of hexamethylcyclopentadiene

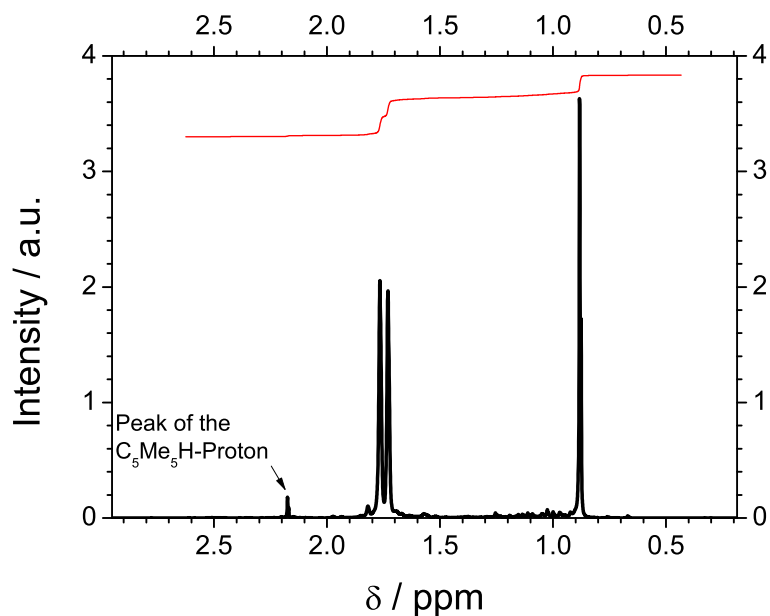


Figure SI.1:  $^1\text{H-NMR}$  spectrum of CPDMe<sub>6</sub> (black). Additionally, the integral of the spectrum (red) is shown. The peak originating from the proton of remaining CPDMe<sub>5</sub>H is labeled.

The synthesis of hexamethylcyclopentadiene (CPDMe<sub>6</sub>) was conducted according to Ref. 1. In short: 1,2,3,4,5-pentamethylcyclopentadiene (Aldrich, purity: 95 %) was deprotonated by sodium amide in liquid ammonia at  $-47\text{ }^\circ\text{C}$ . Afterwards, the anion was methylated by methyl iodide slightly below the boiling point of ammonia. It was extracted by THF and dried over  $\text{MgSO}_4$ . The solvent was evaporated and the crude product was purified by vacuum distillation. It was characterized by UV-Vis and  $^1\text{H-NMR}$  spectroscopy. In the  $^1\text{H-NMR}$  spectrum in Fig. SI.1 the peak originating from the proton ring substituent of the reactant CPDMe<sub>5</sub>H at  $\delta = 2.18$  is labeled. By comparing its integral with the one of the peak at  $\delta = 0.88$ , which originates from the two methyl substituents at the  $\text{sp}^3$  carbon of CPDMe<sub>6</sub>, the purity can be estimated to be  $> 90\%$ .

### Absorption spectrum of CPDMe<sub>4</sub>PrH

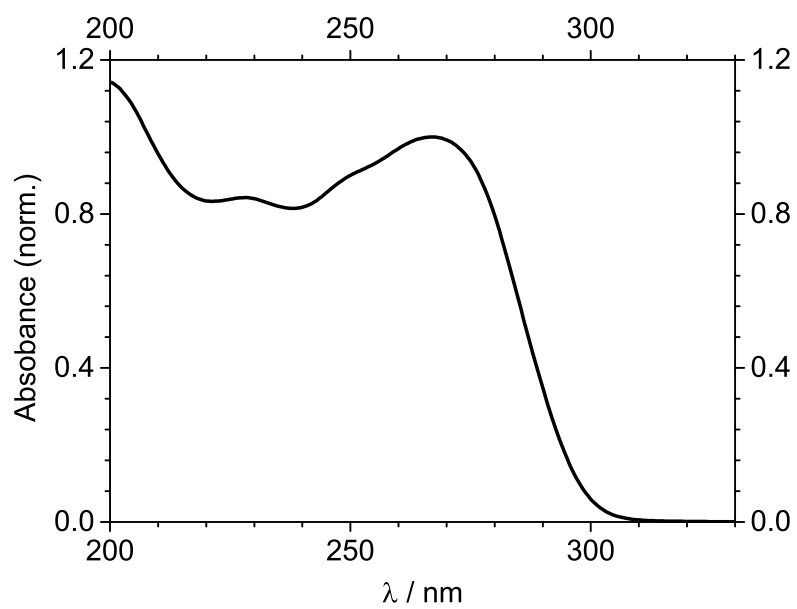


Figure SI.2: Absorption spectrum of CPDMe<sub>4</sub>PrH in cyclohexane.

## Population density evolution

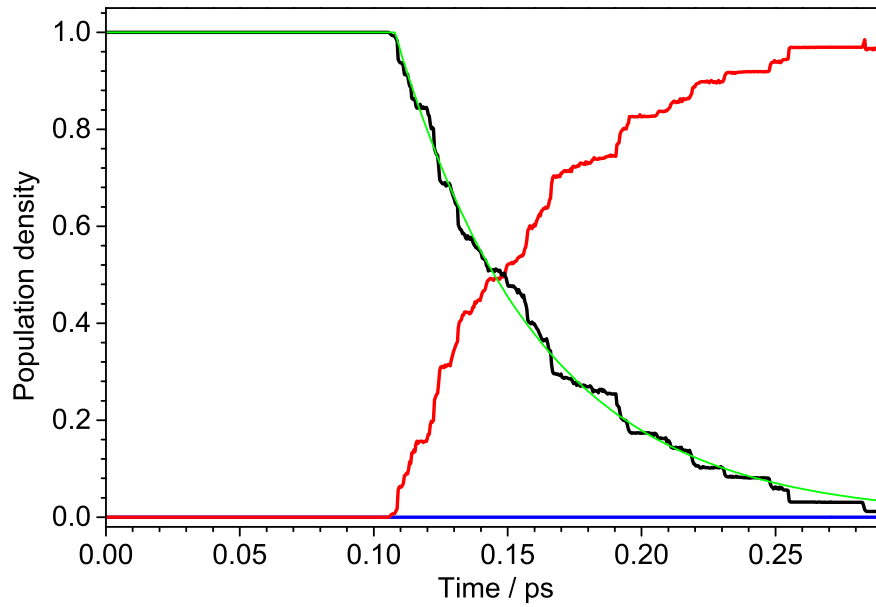


Figure SI.3: Time evolution of population density in  $S_1$  (black),  $S_2$  (blue) and  $S_0$  (red) resulting from the AIMS simulations. Population transfer almost exclusively takes place from  $S_1$  to  $S_0$ . Furthermore, a fit of the  $S_1$  population decay (green) by a delayed exponential is included. After a delay of 108 fs, population is transferred with an exponential time constant of 54 fs.

## Comparison of calculated relative energies of CPD and CPDMe<sub>6</sub>

The experimental absorption spectra show a red-shift of the first absorption band of CPDMe<sub>6</sub> by  $\approx 0.3$  eV compared to CPD. This shift cannot be reproduced by the S<sub>1</sub>-S<sub>0</sub> energy gaps calculated for CPD (5.46 eV, see Ref. 2) and CPDMe<sub>6</sub> (5.47 eV) in the Franck-Condon region on the MS-MR-CASPT2 level of theory. Note that in these calculations the methyl groups of CPDMe<sub>6</sub> were fully incorporated. The optimized minimum-energy conical intersection geometries, which show a high structural agreement (see the visualizations in Fig. 1 of the paper), exhibit considerably larger differences in energies (-2.03 eV for CPD<sup>2</sup> and -2.28 eV for CPDMe<sub>6</sub>, both relative to S<sub>1</sub> in the Franck-Condon region). Thus, the experimentally observed lowering of the S<sub>1</sub>-S<sub>0</sub> gap of CPDMe<sub>6</sub> cannot be reproduced in all areas of the excited state potential energy surface by the employed method. For a more accurate description, the complete active space employed in the calculations probably would have to be expanded by molecular orbitals of the methyl group. Since we are already forced by computational complexity to approximate the methyl groups as hydrogens with mass 15, such an expansion is neither feasible nor, as the results show, important for a qualitative agreement of the simulations with experimental findings.

### S<sub>1</sub> wavepacket projections

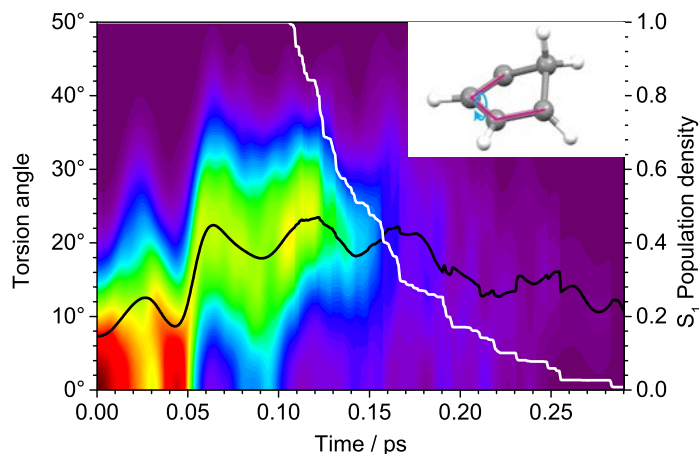


Figure SI.4: Projection of the time evolution of the S<sub>1</sub> wavepacket density onto the ring torsion degree of freedom visualized in the inset. Red corresponds to high density, violet to low density. The time-dependent expectation value of the torsion angle is inserted as a black curve. For comparison, the S<sub>1</sub> population density is also inserted as a white curve. The torsion angle is not Franck-Condon active and thus needs an induction time of about 50 fs to start relaxation to the equilibrium value of about 20°. There is no obvious correlation to the S<sub>1</sub> population density decay.

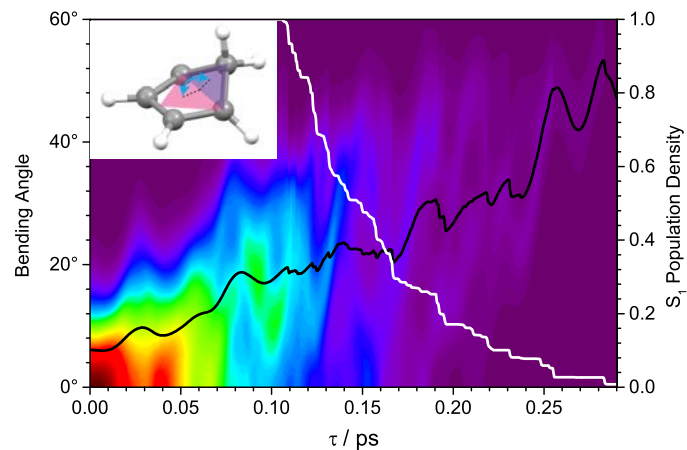


Figure SI.5: As Fig. SI.4, but projection onto the ring bending degree of freedom visualized in the inset. Immediately after time zero, the expectation value of the angle begins to increase without obtaining a new equilibrium value. No correlation to the  $S_1$  population density decay is observable.

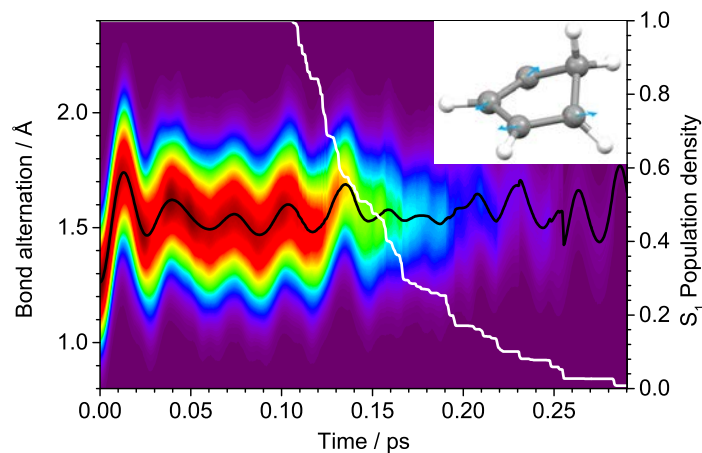


Figure SI.6: As Fig. SI.4, but projection onto the bond alternation degree of freedom visualized in the inset. The degree of freedom is Franck-Condon active since it immediately starts to adopt a new equilibrium value of about 1.5 Ångström, which is not altered by the  $S_1$  population density decay.

Figures/

## Derivation of the stepladder model

The model depicted in Fig. 5 of the paper is essentially a step ladder-type model as used to describe unimolecular reaction kinetics of highly excited species, but was already derived previously for the case of excited state molecular dynamics<sup>3</sup>.

The step with the highest energy can be associated with the FC region of  $S_1$ , the lowest step can be understood as the CoIn region of  $S_1$  from where population transfer to  $S_0$  can take place. The steps are assumed to exhibit a uniform energy spacing. The statistical probability for population density to be transferred to the next lower step is, furthermore, characterized by unimolecular kinetics employing an uniform time constant  $\tau_s$ . The probability for back-transfer to the next higher step is set to zero. The latter is justified in this case since the dynamics simulations indicate no evidence of equilibrium conditions for the  $S_1$  population during relaxation.

Time-dependent distribution of the population density over the steps can be evaluated with a scheme of coupled differential equations each describing the time-dependent population of a single step. The coupled equations are subject to the boundary condition that at  $t=0$  only the Franck-Condon state (step 0) is populated. As pointed out in detail in Ref. 3, the general expression for the population density evolution  $P_j(t)$  in any step  $j$  up to the final state (i.e. in the present context any step on  $S_1$ ) is

$$P_j(t) = \frac{t^j}{j! \tau_s^j} e^{-\frac{t}{\tau_s}}. \quad (1)$$

The population of the final state rises with time, as given by Eq. 12c in Ref. 3. The overall population of transiently visited states can be expressed as

$$P_{S_1}(t) = e^{-\frac{t}{\tau_s}} \sum_{j=0}^n \frac{t^j}{j! \tau_s^j}. \quad (2)$$

A plot of Eq. 2 vs. the time is always – except for  $n=0$  – characterized by a plateau at  $P_{tot}(t=0)$  followed by an S-shaped decay to zero. The characteristic time  $t_{ch}$ , where the decay takes place is well represented by the inflection point of the S-shaped decay

$$\frac{d^2 P_{tot}(t_{ch})}{dt_{ch}^2} = e^{-\frac{t_{ch}}{\tau_s}} \left[ \frac{t_{ch}^n - t_{ch}^{n-1} n \tau_s^{-1}}{n! \tau_s^{n+2}} \right] = 0 \quad (3)$$

$$t_{ch} = n \cdot \tau_s \quad (4)$$

## Fit of the CPDMe<sub>6</sub> data with the model

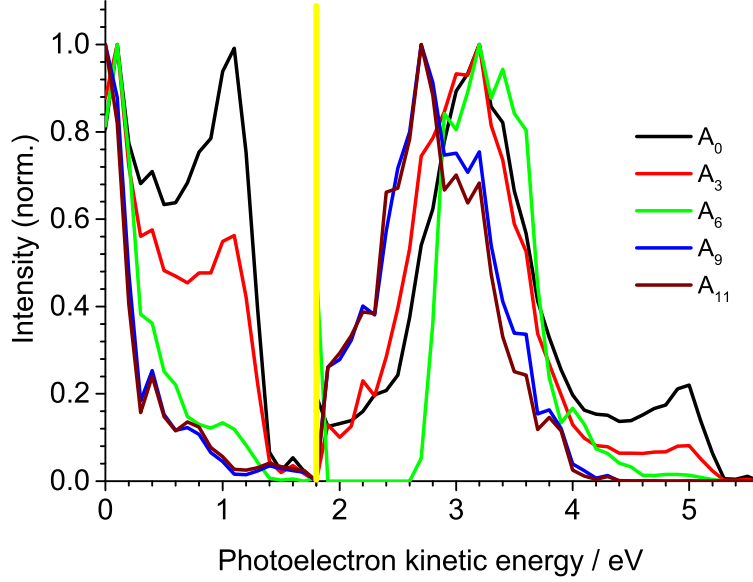


Figure SI.7: Selected spectral signatures  $A_j$  from a fit of the simulated time-resolved photoelectron spectra with Eq. 4 of the paper employing  $n = 11$  and  $\tau_s = 13$  fs. The  $A_j$  are normalized with respect to their maxima in the one-photon ionization and the two-photon ionization regime.

Experimental time-resolved photoelectron spectra were cut into slices of  $\Delta E \approx 0.07$  eV and fitted with Eq. 4 of the paper employing  $n = 11$ . Accordingly,  $\tau_s$  is treated as a fit parameter. Its value is obtained to be  $(49 \pm 3)$  fs and  $t_{ch}$   $(540 \pm 30)$  fs. In contrast to the simulated spectra, the experimental data contain noise. Thus, for better comparison with the trends in Fig. SI.8, three adjacent amplitude spectra were added up.

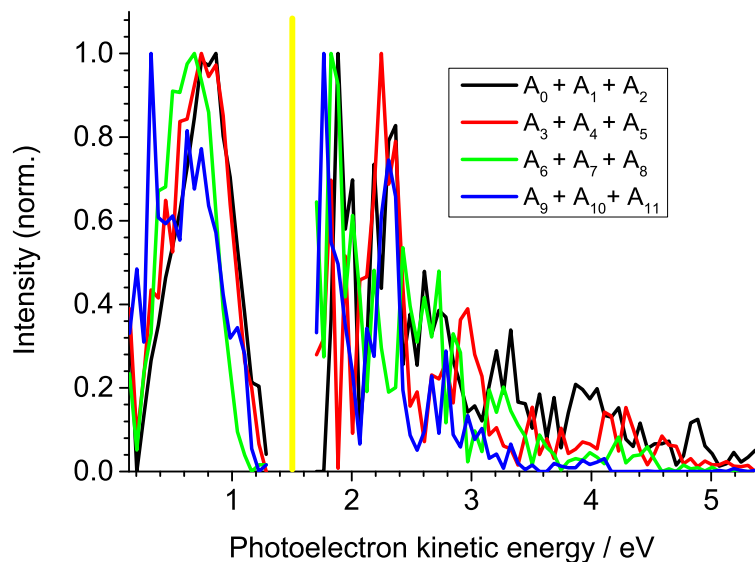


Figure SI.8: Spectral signatures  $A_j$  from a fit of the experimental TRPES spectrum with Eq. 4 of the paper employing  $n = 11$ . For an improved visualization, three consecutive signatures are added and normalized with respect to their maxima in the one-photon ionization and the two-photon ionization regime.

## References

- [1] L. de Vries, *J. Org. Chem.*, 1960, **25**, 1838.
- [2] T. S. Kuhlman, W. J. Glover, T. Mori, K. B. Møller and T. Martínez, *Faraday Discuss.*, 2012, **157**, 193–212.
- [3] K. B. Møller and A. H. Zewail, *Chem. Phys. Lett.*, 2002, **351**, 281.